Atmospheric Environment 78 (2013) 259–267

Contents lists available at SciVerse ScienceDirect

Atmospheric Environment

journal homepage: www.elsevier.com/locate/atmosenv

Estimated range of black carbon dry deposition and the related snow albedo reduction over Himalayan glaciers during dry pre-monsoon periods

Teppei J. Yasunari [a,b,*], Qian Tan [a,b], K.-M. Lau [a], Paolo Bonasoni [c,d], Angela Marinoni [c], Paolo Laj [e], Martin Ménégoz [e], Toshihiko Takemura [f], Mian Chin [a]

[a] NASA Goddard Space Flight Center, Greenbelt, MD, USA
[b] Goddard Earth Sciences and Technology and Research, Universities Space Research Association, Columbia, MD, USA
[c] CNR – Institute for Atmospheric Sciences and Climate, Bologna, Italy
[d] Ev-K2-CNR Committee, Bergamo, Italy
[e] Laboratoire de Glaciologie et Géophysique de l'Environnement, Université Grenoble 1 – CNRS (UMR5183), St Martin d'Heres, France
[f] Research Institute for Applied Mechanics, Kyushu University, Fukuoka, Japan

ARTICLE INFO

Article history:
Received 4 October 2011
Received in revised form
7 March 2012
Accepted 9 March 2012

Keywords:
Biomass burning
Himalayas
Black carbon
Deposition
Snow melting

ABSTRACT

One of the major factors attributed to the accelerated melting of Himalayan glaciers is the snow darkening effect of atmospheric black carbon (BC). The BC is the result of incomplete fossil fuel combustion from sources such as open biomass burning and wood burning cooking stoves. One of the key challenges in determining the darkening effect is the estimation uncertainty of BC deposition (BCD) rate on surface snow cover. Here we analyze the variation of BC dry deposition in seven different estimates based on different dry deposition methods which include different atmospheric forcings (observations and global model outputs) and different spatial resolutions. The seven simulations are used to estimate the uncertainty range of BC dry deposition over the southern Himalayas during pre-monsoon period (March–May) in 2006. Our results show BC dry deposition rates in a wide range of 270–4700 μg m^{-2} during the period. Two global models generate higher BC dry deposition rates due to modeled stronger surface wind and simplification of complicated sub-grid surface conditions in this region. Using ice surface roughness and observation-based meteorological data, we estimate a better range of BC dry deposition rate of 900–1300 μg m^{-2}. Under dry and highly polluted conditions, aged snow and sulfate-coated BC are expected to possibly reduce visible albedo by 4.2–5.1%. Our results suggest that for estimating aerosol-induced snow darkening effects of Himalaya snowpacks using global and regional models, realistic physical representation of ice or snow surface roughness and surface wind speed are critical in reducing uncertainties on the estimate of BC deposition over snow surface.

1. Introduction

Atmospheric black carbon (BC), also known as soot, is a strong absorber of solar radiation in the atmospheric particulate phase (Bond and Bergstrom, 2006; IPCC, 2007). Recent studies show that BC coated by other aerosols, such as sulfate, after its emission into the atmosphere has even larger absorbing power than non-coated BC (e.g., Redemann et al., 2001; Schwarz et al., 2008; Naoe et al., 2009). China and India are large emission sources of BC from industry, residential, and transport sectors, including the incomplete fossil fuel combustion from sources such as open biomass burning, and wood burning cooking stoves (Bond et al., 2004; Ramanathan et al., 2007; Ramanathan and Carmichael, 2008). Of interest to this study are the intense emissions of BC from biomass burning activities (forest fires, agricultural practices, wood cooking fires) on the Indo-Gangetic Plain. Biofuel cooking, alone, emits more than 1800 tons of BC annually in the region (Ramanathan and Carmichael, 2008). Its impacts on the Himalayan glaciers are considered to be significant. The high concentration of BC over the region heats the atmosphere and may lead to atmospheric water cycle feedback through the so-called *Elevated Heat Pump* (EHP) during the pre- and early monsoon seasons (Lau et al., 2006). The EHP modifies the energy balance between the atmosphere and the land over northern India and the Himalayas-Tibetan Plateau (TP) region, potentially changing the precipitation pattern of the Indian monsoon (Lau et al., 2006, 2008; Lau and Kim, 2006) and

* Corresponding author. Goddard Earth Sciences and Technology and Research, Universities Space Research Association, Columbia, MD, USA.
E-mail address: teppei.j.yasunari@nasa.gov (T.J. Yasunari).

1352-2310/$ – see front matter © 2012 Elsevier Ltd. All rights reserved.
doi:10.1016/j.atmosenv.2012.03.031

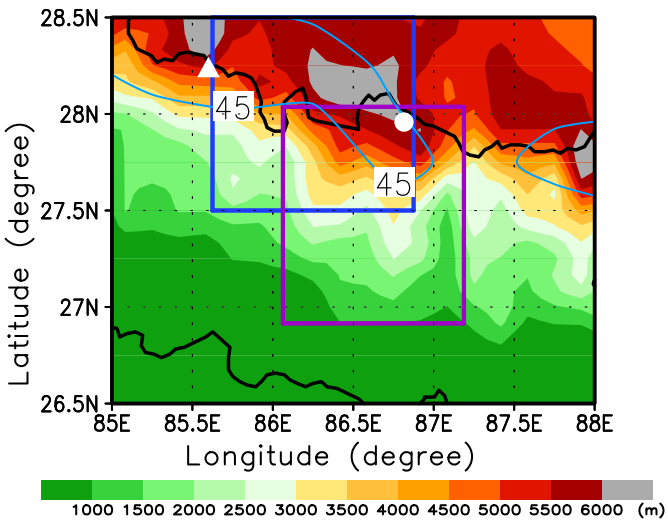

Fig. 1. Map of the study area. White triangle and circle denote the location of Yala Glacier and NCO-P site, respectively. The squares in blue and purple are one grid point of GOCART and SPRINTARS, respectively. The curved sky blue lines are mean snow water equivalent for March–May in 2006 of more than 45 mm by AMSR-E data (Tedesco et al., 2004) indicating the areas including glaciers. The Merged IBCAO/ETOPO5 Global Topographic Data Product by Holland (2000) was used for topography map.

accelerating the spring melting of Himalayan snowpack (Lau et al., 2010). The high BC emissions, extending up to the Himalayan glaciered regions, are significant because the snow darkening effect decreases the snow surface albedo (Warren and Wiscombe, 1980; Flanner et al., 2007, 2009; Yasunari et al., 2011; Aoki et al., 2011) and is likely causing glacier retreats (Flanner et al., 2007; Menon et al., 2010; Qian et al., 2011; Ming et al., 2012). In fact, direct observations of these high BC concentrations (BCC) in the atmosphere during pre-monsoon seasons have been detected at the Nepal Climate Observatory – Pyramid (NCO-P) in the form of brown clouds (Bonasoni et al., 2008, 2010; Marinoni et al., 2010). The brown clouds consist of absorbed anthropogenic aerosols such as BC. The BC both absorbs and scatters solar radiation and has significant influence on Aerosol Optical Depth (AOD) >0.3 (Ramanathan et al., 2007). The local radiative forcing due to BC can be greater than 10 W m^{-2} during pre-monsoon period (Marcq et al., 2010).

During the pre-monsoon period (April through the first part of June) of 2006, very little precipitation had been observed at the NCO-P (Bonasoni et al., 2010; Yasunari et al., 2010), and BC is considered to essentially be removed from the atmosphere by dry deposition. Hence, we focus on dry deposition during pre-monsoon season in this analysis. Yasunari et al. (2010) estimated the lower bound BC dry deposition (BCD) over the southern parts of the Himalayas in the pre-monsoon season and its "lower bound" albedo reductions over Himalayan glaciers were possibly 2.0–5.2%. A fixed small dry deposition velocity (v_d) of 1.0×10^{-4} m s^{-1} was assumed. In reality, the influence of snow albedo reductions is expected to be greater over non-debris-covered parts of Himalayan glaciers (See Supplementary Information, hereafter called SI). We know the diurnal cycle of meteorological components such as wind speed and temperature, and the fluctuations of the other meteorological components such as relative humidity, affecting the micro-meteorological conditions near the surface. Because of these factors, the day time v_d should be faster than the lower bound v_d assumed in Yasunari et al. (2010). It can increase BCD more than that estimated with the lower bound v_d.

Table 1
Surface roughness height for calculations.

	[m]
Cases 2, 4, and 5 (ice surface)	0.0001
Case 3 (conifer surface)	1.0000
Case 6 (based on tundra [15%], conifer [20%], desert [50%], and shrub/grass [15%])	0.0463 ± 0.0004
Cases 7 (based on broadleaf deciduous forest & woodland)	0.1287 ± 0.0029

Note: For Cases 2–5, surface roughness data were obtained from the GOCART surface roughness table. For cases 6 and 7, mean surface roughness and standard deviation for March–May in 2006 are shown.

Factors controlling snow melt and glacier mass balance are complex. They are linked to local temperature variability, debris-covered area, heat balance, including snow darkening effects, and precipitation (e.g., Fujita and Ageta, 2000; Fujita, 2008; Scherler et al., 2011; Yasunari, 2011, and references therein). Contributors to the snow darkening, such as BC, dust, organic matters, and snow algae deposited in snow, may alter the snow melt rate via snow albedo changes (e.g., Takeuchi et al., 2001; Flanner et al., 2007; Flanner et al., 2009; Yasunari et al., 2011; Aoki et al., 2011). Each factor has its own uncertainty and those uncertainties should be reduced for more accurate discussion on the glacier issues. Here, in this study, we focus on one of the factors, BC, because deposits from biomass burning and other anthropogenic sources in Indo-Gangetic Plain are expected to be significant over the foothills of the Himalayas.

Very limited observations of BC in/above snow cover in terms of concentration and morphology over Himalayan and Tibetan regions have been carried out (Cong et al., 2009, 2010; Kaspari et al., 2011; Ming et al., 2008, 2009; 2012; Xu et al., 2006, 2009a; 2009b). These studies are, for the most part, completed over the northern slope of Himalayas or Tibetan Plateau. Few studies of the snow-BC-related

Table 2
Summary of estimated deposition velocity, BC dry deposition (BCD), and BC concentrations (BCC) in the snow surface.

Cases	Dry deposition velocity (DDV) (m s^{-1})			Total BCD (MAM)	BCC (Top 2-cm snow)	BCC (Top 2-cm snow)
					Snow density (110 kg m^{-3})	Snow density (500 kg m^{-3})
	Max	Min	Mean	μg m^{-2}	μg kg^{-1}	μg kg^{-1}
1: Fixed DDV + met-data 1	1.00E-04	1.00E-04	1.00E-04	266	120.8	26.6
2: GOCART DDV code + met-data 1 (ice surface)	4.10E-03	1.00E-04	5.40E-04	1333	605.9	133.3
3: GOCART DDV code + met-data 1 (conifer surface)	1.19E-02	1.00E-04	1.82E-03	4651	2114.2	465.1
4: MOCAGE DDV + met-data 1 (ice surface)	2.59E-03	1.00E-04	3.55E-04	916	416.2	91.6
5: MOCAGE DDV + met-data 1 without terminal velocity (ice surface)	2.57E-03	1.00E-04	3.48E-04	896	407.4	89.6
6: GOCART/GEOS-4 output (Model; vegetated surface)	5.20E-03	1.09E-04	1.71E-03	3852	1751.1	385.2
7: SPRINTARS output (Model; vegetated surface)	1.95E-03	1.72E-04	1.76E-03	4361	1982.2	436.1
Difference among cases 1–7	1.18E-02	7.20E-05	1.72E-03	4385	1993.4	438.5

Note: All the estimates in Cases 1–5 excluded the time period when the 1-hourly mean equivalent BC concentrations were not available. The DDV and total BCD for Case 1 were obtained from Yasunari et al. (2010).

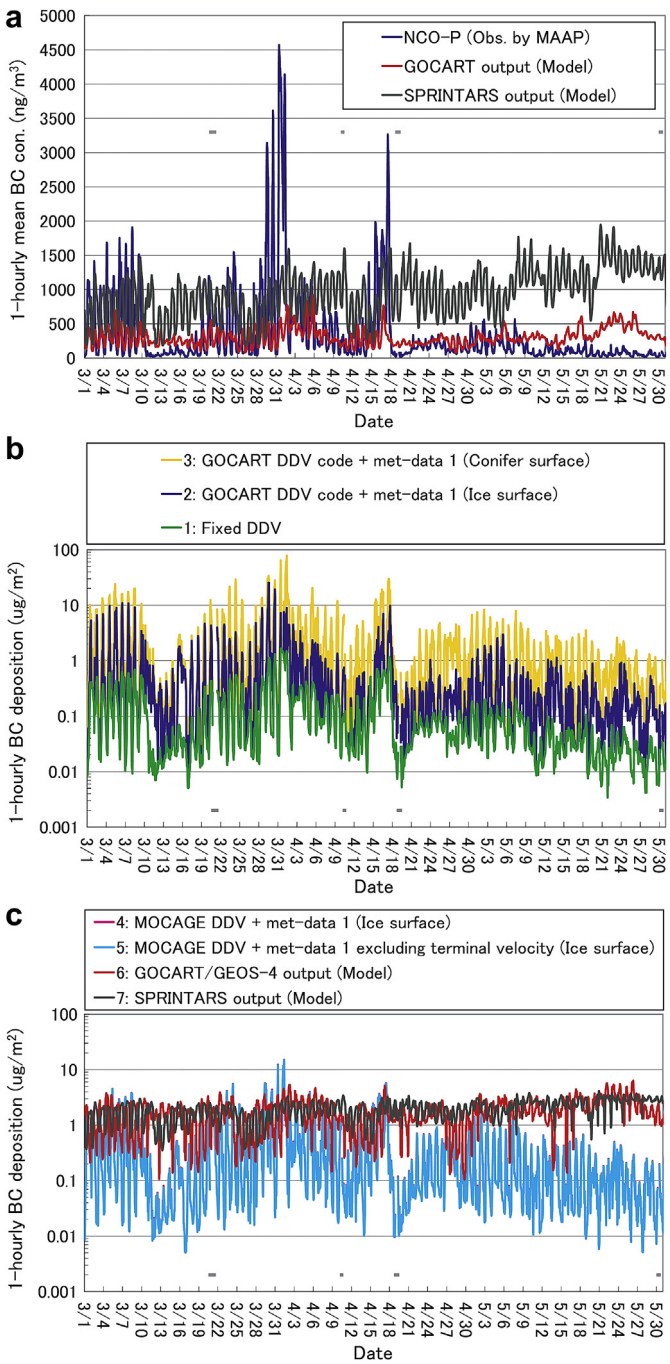

Fig. 2. (a) 1-hourly mean BCC in air by the MAAP observations at NCO-P (eqBCC: Bonasoni et al., 2008; Marinoni et al., 2010), GOCART (Case 6), and SPRINTARS (Case 7). (b) 1-hourly total deposition amount of BC estimated from the MAAP data at NCO-P with the various dry deposition velocity (DDV: v_s) (Cases 1–3; Case 1 by Yasunari et al., 2010). (c) Same as (b) but for Cases 4 and 5, GOCART (Case 6), and SPRINTARS (Case 7). The time is in UTC. The horizontal lines in gray in the figures (a)–(c) denote the time period for which eqBCC data were not available and not used for analysis.

issues have been carried out over the southern slope (Yasunari et al., 2010). The difficulties in accessing these mountain regions limit direct observations. In addition, there have not had enough direct atmospheric observations on continuous BCD (i.e., time series of BCD) over the snow surface of Himalayan glaciers. Because the area is so remote, alternate methods of estimating BCD over this vulnerable region, such as using global and regional models, are critical to the studies of snow albedo reductions and glacier melting.

The chemical transport model (CTM) provides useful spatial information on BCD (e.g., Takemura et al., 2000; Chin et al., 2002; Flanner et al., 2007; Qian et al., 2009, 2011). However, the model includes assumptions and uncertainties in their estimations. The uncertainty of the CTM-estimated dry deposition rate is related to assumptions of dry deposition scheme, turbulent scheme, and sub-grid scale inhomogeneities including topography, land surface use, surface roughness, etc. Hence, we examine the impact of model uncertainties on the estimation of the uncertainty range (i.e., how wide range it possibly has) of BCD and its related snow albedo reductions over Himalayas. This examination is essential if we are to assess the BCD from the anthropogenic sources in Indo-Gangetic Plain to the Himalayas.

The aim of this study is to estimate the possible uncertainty range of total BCD within the different estimates during dry pre-monsoon period in 2006 and its relevant snow albedo reductions at locations on the southern foothill over the Himalayas, because dry deposition is the major pathway for anthropogenic BC to contaminate Himalayas glaciers during this highly polluted period. We will use five different cases of dry deposition velocities (v_d) based on Yasunari et al. (2010), calculations from NCO-P observations with dry deposition schemes, and outputs from two global model simulations. Because there are no available in situ direct observations of BC dry deposition velocity (v_d) and BCD over glaciers at the southern slope of Himalayas, currently we cannot carry out any validation studies. Future observation can validate this point. In this mostly modeling-based study, we try to estimate the lower and higher bound of uncertainty covering a wider range of conditions. We hope this estimate will encourage ballpark glacier melting studies and inspire more detailed observational and modeling studies.

In Section 2, we described the observation and model data used in this analysis, and calculation of 7 sets of dry deposition velocity (v_d). The differences between v_d, BC deposition, BC concentrations, and snow albedo reductions are discussed in Sections 3. We try to identify what contributes to those large disparities and then summarize the study in Section 4.

2. Method and data

2.1. Comparisons of black carbon concentrations in the atmosphere and depositions

In this study, we used seven different methods to estimate BCD using different v_d and model outputs. Basically, the BCD amount is calculated as $C_{air} \times v_d \times t$, where C_{air}, v_d, and t are BC concentration in the atmosphere, dry deposition velocity, and total time in seconds, respectively. Multiple observations have been made at the NCO-P station on the southern slope of the Himalayas during pre-monsoon season (March–May) in 2006, including equivalent BC atmospheric concentration (eqBCC) (Marinoni et al., 2010) (See SI), and meteorological parameters, obtained from the NCO-P Global GAW Station (5079 m a.s.l.) (Bonasoni et al., 2008, 2010) in the high Khumbu valley (Fig. 1). Those meteorological data with eqBCC were used for the calculation of v_d and BCD calculations, in which some variables are calculated, assuming Yala glacier conditions mentioned in Yasunari et al. (2010) and SI. Hereafter, we call these data: met-data 1.

We also used outputs from two global chemistry transport models at the grid point including the NCO-P site. The first model used is the Goddard Chemistry Aerosol Radiation and Transport (GOCART) model (e.g., Chin et al., 2002, 2009) (See SI). The second is the Spectral Radiation-Transport Model for Aerosol Species (SPRINTARS) (Takemura et al., 2000, 2002) (See SI).

Finally, seven cases of BC depositions during the pre-monsoon 2006 (March–May; MAM) were calculated. To estimate the uncertainty ranges in seven estimates, we used different dry deposition models including sensitivity tests to examine the effects of surface roughness

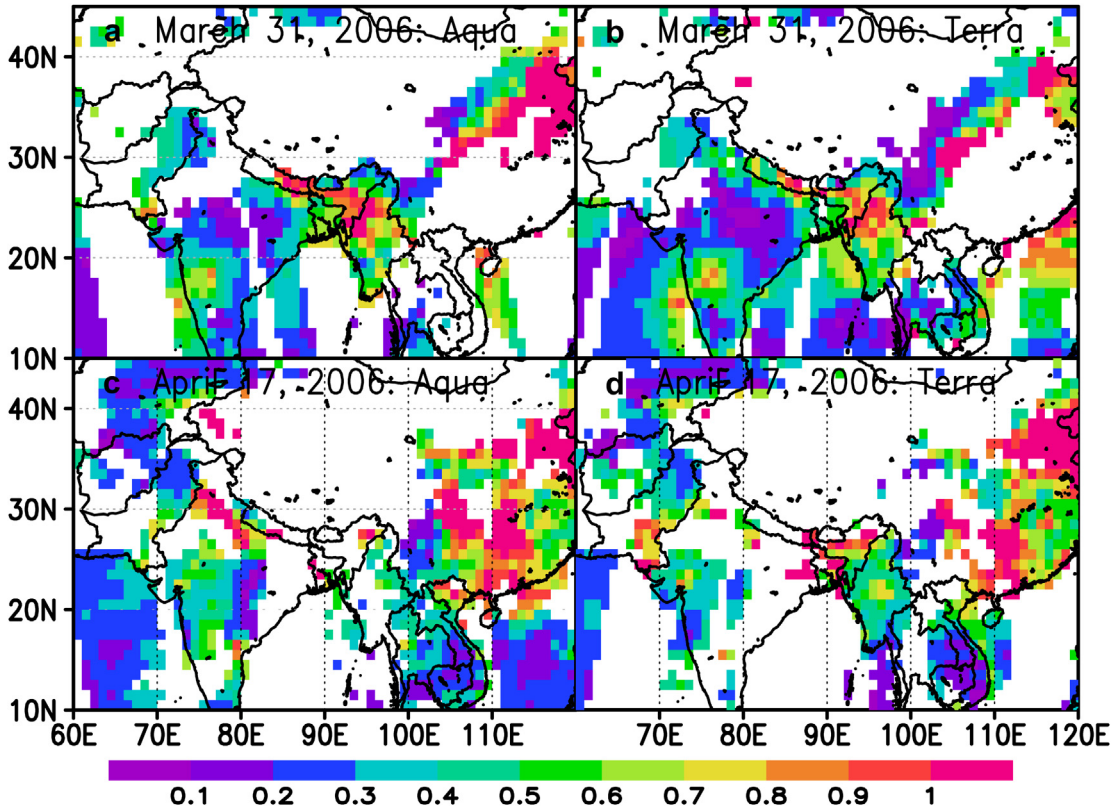

Fig. 3. MODIS Aerosol Optical Depth at 550 nm for the BC events on March 31 (a: Aqua; b: Terra) and April 17 (c: Aqua; d: Terra) in 2006 in Fig. 2. The data were obtained from Giovanni (available at: http://disc.sci.gsfc.nasa.gov/giovanni).

change and the effect of gravity settling by submicron particles on the deposition velocity estimates. In addition, we used simulations from two global models. The estimated 1-hourly mean dry deposition velocities were used to estimate 1-hourly BCD amount ($=$ eqBCC $\times$ v_d $\times$ 3600 s). The calculations were done from March 1 to May 31 in Coordinated Universal Time (UTC).

1) The dry deposition amount estimated with a fixed v_d of 1.0×10^{-4} m s^{-1} by Yasunari et al. (2010).
2) The 1-hourly mean v_d was calculated by the same dry deposition velocity scheme used in GOCART in GEOS-4 model (Case 6) forced by met-data 1 and the additional inputs calculated from the met-data 1 (See SI) together with an assumed ice

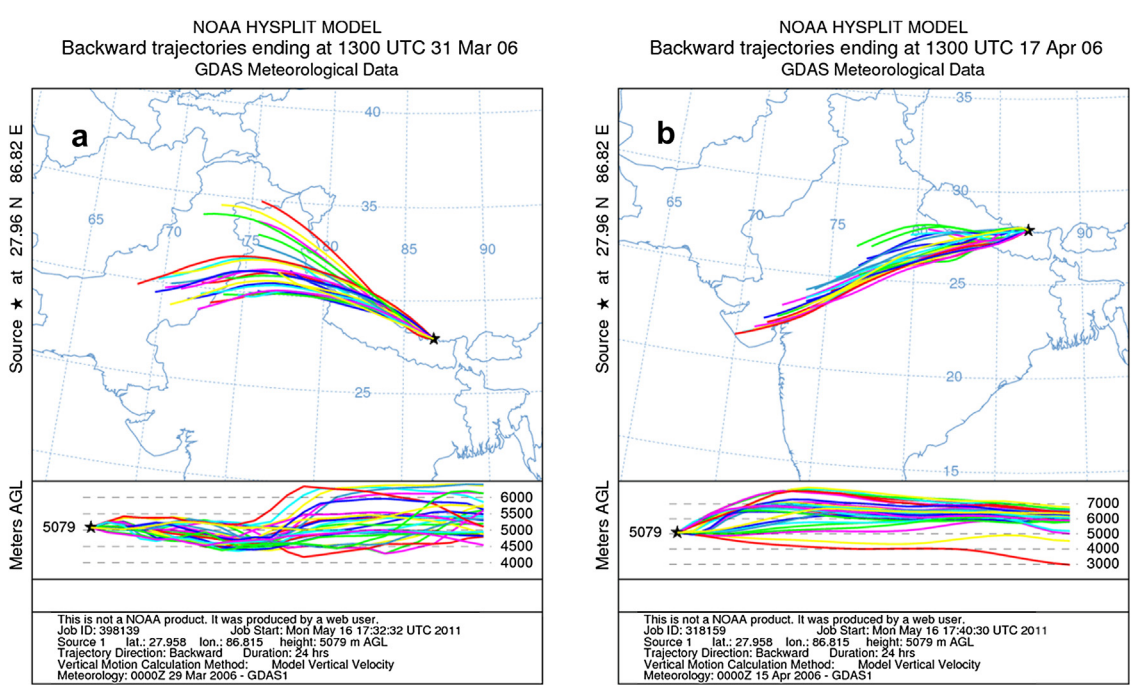

Fig. 4. Backward trajectories (ensemble) simulated by NOAA HYSPLIT ending at (a) 13:00UTC on March 31, 2006, and (b) 13:00UTC on April 17, 2006.

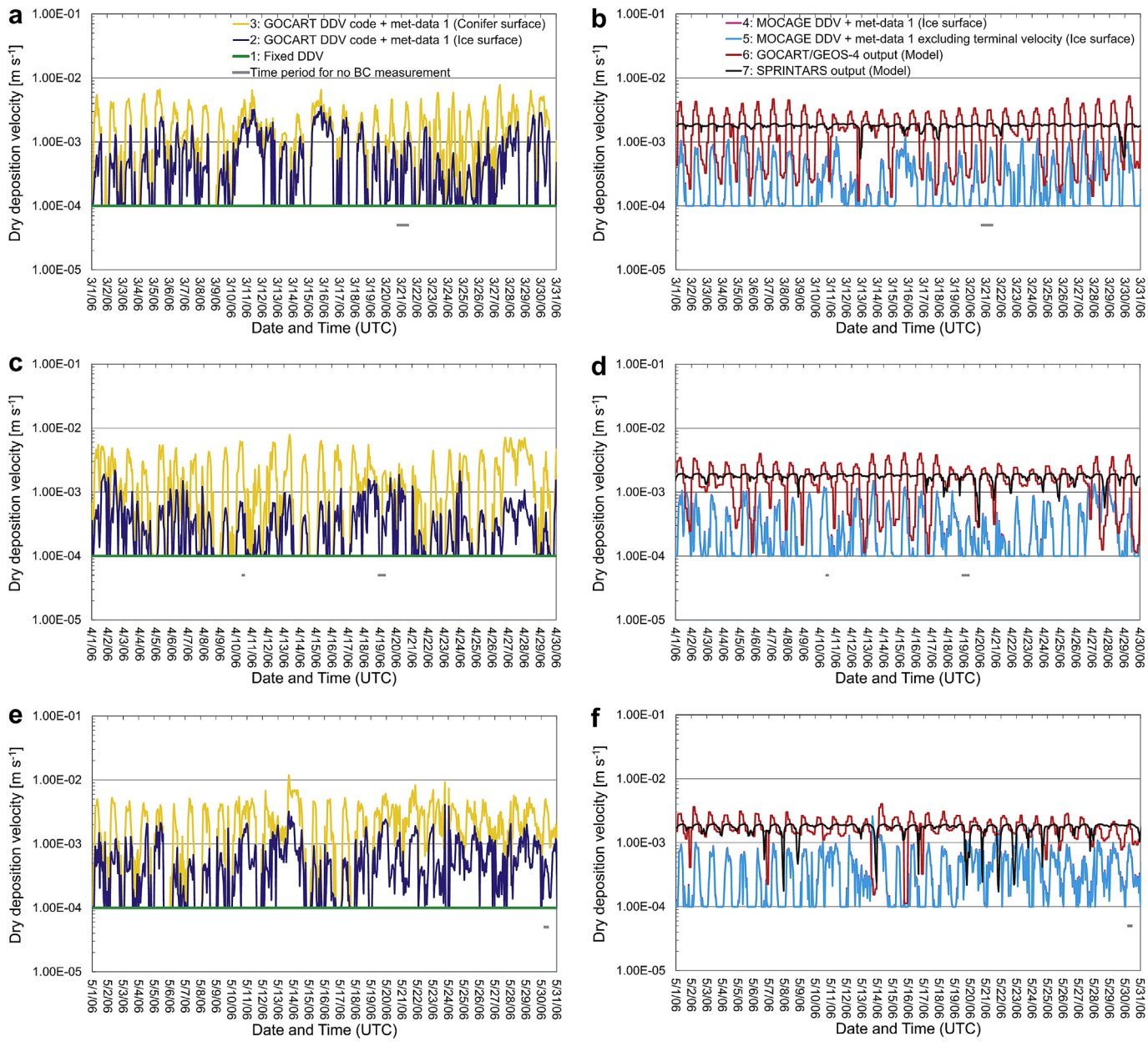

Fig. 5. 1-hourly mean dry deposition velocities (DDV: v_d) for Case 1–3 (a, c, and e; Case 1 from Yasunari et al., 2010) and 4–7 (b, d, and f) on March (1st row), April (2nd row), and May (3rd row). The horizontal lines in gray in the figures (a)–(c) denote the time period for which the eqBCC data (Bonasoni et al., 2008; Marinoni et al., 2010) were not available and not used for analysis.

surface leading to a surface roughness height of 1.0×10^{-4} m (Table 1).

3) Same as (2), except for an assumed conifer surface giving "a larger surface roughness height" of 1.0 m (Table 1).
4) The 1-hourly mean v_d was calculated by another deposition velocity theory by Nho-Kim et al. (2004) forced by met-data 1, and the additional inputs calculated from the met-data 1, together with the ice surface assumptions in Table 1 and used to estimate a 1-hourly BCD amount. The deposition velocity equation also considers the gravity settling effect (See SI).
5) As same as (4), but the term on terminal velocity (v_s) of particles in equation (1) by Nho-Kim et al. (2004) was ignored to remove the gravity settling effect of particles.
6) The output data of 1-hourly BCD amount at the grid point corresponding to NCO-P site (Fig. 1; 28°N, 86.25°E; 3511.27 m a.s.l.) by GOCART off-line simulation in GEOS-4 were used for comparisons. The GOCART used Walcek et al. (1986) and Wesely (1989) dry deposition schemes. At 1° × 1.25° grid cell containing the location of NCO-P, the vegetation types of land surface in GEOS-4 were defined as a vegetation mixture of tundra (15%), conifer (20%), desert (50%), and shrub/grass (15%) with no ice surface (Table 1).
7) The output data of 1-hourly BCD amount by SPRINTARS online simulation in AORI/NIES/JAMSTEC AGCM with broadleaf deciduous forest and woodland surface type at the grid point corresponding to NCO-P site (Fig. 1; 27.476°N, 86.625°E; 2510 m a.s.l.) were used for comparisons. The SPRINTARS calculated carbon depositions as internal mixture of BC and OC. Hence, BCD was estimated as follows; Total BCD = (BC + OC depositions) × (Total column mass of BC)/(Total column mass of BC + OC).

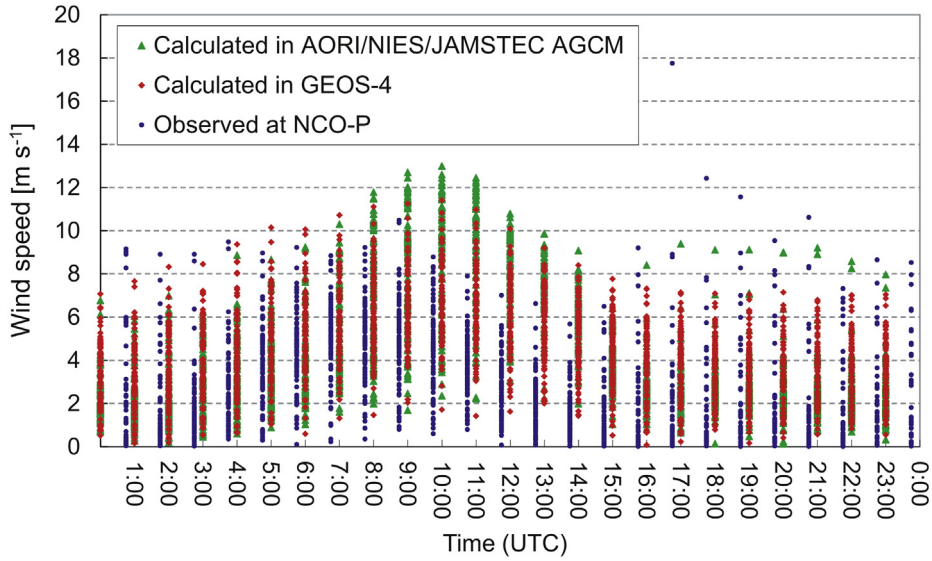

Fig. 6. Comparisons of mean surface wind velocities at the location of NCO-P site and the grid points which include the NCO-P site among the observed data at NCO-P based on Bonasoni et al. (2008) (1-hourly), the simulated data in GEOS-4 (used for GOCART; 1-hourly; Case 6), and the simulated data in AORI/NIES/JAMSTEC AGCM (used for SPRINTARS; 1-hourly; Case 7).

2.2. Snow albedo changes estimated with different BCD

We estimated how much snow albedo reduction is likely to occur due to the differences in the estimation of BCDs. The snow albedo reductions from pure snow albedo, due to the estimated BCDs from 7 cases, were computed based on the calculations by the snow albedo model of Yasunari et al. (2011) (See SI).

3. Results and discussion

3.1. Differences of BCC and BCD

We estimated BCD from 7 cases including different dry deposition velocity theories, settings, and outputs from global models (Table 2). In Fig. 2, 1-hourly mean BCC in the atmosphere and total BCD were shown. The BCC in the atmosphere simulated by GOCART in GEOS-4 (Case 6) reproduced the background level of the observed eqBCC at NCO-P site, but this is probably due to faster v_d as mentioned later. The SPRINTARS (Case 7) overestimated by a factor of 2.8 compared to observations at NCO-P in terms of 3-monthly mean. Both the model simulations failed to reproduce two large BC peaks (Fig. 2a). Those observed eqBCC peaks were better explained by higher AOD seen in the Moderate Resolution Imaging Spectroradiometer (MODIS) data and the air mass transport patterns by NOAA HYSPLIT model outputs (ensemble backward trajectories) (Draxler and Rolph, 2011; Rolph, 2011). The peak AOD on March 31 was from the emission source with higher AOD in Nepal and effects of diurnal mountain breeze, while low AOD was found in the Indo-Gangetic Plain (Figs. 3a, 3b, and 4a). The other peak on April 17 was probably due to higher AOD in IGP with regional air mass transport to NCO-P site (Figs. 3c, 3d, and 4b).

The time evolution characteristics for BCD fluctuations in Cases 1–5 depended on v_d and the observed eqBCC in the atmosphere which were prescribed the same in all these cases (see Section 2.1). Hence, although absolute BC deposition rates were different, similar fluctuations of BCD were seen for Cases 1–5 (Fig. 2b and c). If local eqBCC increases, the related BCD amount also increases for Cases 1–5. The simulated BCDs by GOCART (Case 6) and SPRINTARS (Case 7) were much higher compared to the Cases 1, 2, 4, and 5. The

Table 3
VIS and NIR snow albedos for hydrophobic and hydrophilic BCs in new and old snow.

	Hydrophobic BC				Hydrophilic BC			
	New snow		Old snow		New snow		Old snow	
	Snow density (110 kg m^{-3})		Snow density (500 kg m^{-3})		Snow density (110 kg m^{-3})		Snow density (500 kg m^{-3})	
	VIS	NIR	VIS	NIR	VIS	NIR	VIS	NIR
Pure snow	0.981	0.669	0.954	0.515	0.981	0.669	0.954	0.515
Case 1	0.969	0.667	0.932	0.514	0.964	0.666	0.924	0.513
Case 2	0.954	0.663	0.918	0.510	0.942	0.660	0.903	0.508
Case 3	0.911	0.648	0.877	0.500	0.880	0.639	0.845	0.493
Case 4	0.960	0.664	0.924	0.512	0.951	0.662	0.911	0.510
Case 5	0.960	0.664	0.924	0.512	0.951	0.662	0.912	0.510
Case 6	0.921	0.652	0.887	0.502	0.894	0.644	0.858	0.497
Case 7	0.914	0.649	0.881	0.501	0.885	0.641	0.850	0.494
MIN	0.911	0.648	0.877	0.500	0.880	0.639	0.845	0.493
MAX	0.969	0.667	0.932	0.514	0.964	0.666	0.924	0.513
DIFF (%)	5.8	1.9	5.5	1.4	8.4	2.7	7.9	2.0

Note: Values underlined denote the most likely range of snow albedos we discussed during March–May 2006 in aged snow. The DIFF means the difference between MIN and MAX within Cases 1–7.

global models also could have not reproduced two BC peaks (Fig. 2a and c). The highest BCD was obtained in Case 3, which used the greatest surface roughness height of conifer so as to compare with the roughness of ice surface (Table 1). What is interesting here is Case 3 did exceed the estimates from the global models in Cases 6 and 7. This finding indicates the importance of using proper surface roughness on the deposition velocity calculation.

3.2. Differences of dry deposition velocity

There are large differences in the estimates on v_d (Table 2 and Fig. 5). We also additionally compile available v_d for submicron-dominated particles at the many places in the cryosphere as reference (SI and Table S1). The observation based v_d over ice/snow in the previous studies having wide range of 10^{-5}–10^{-2} m s^{-1} but often seen in the dominant velocity order of 10^{-4} m s^{-1} is similar to our estimates in Table 2. It indicates that our estimates are within the range of v_d over ice/snow surface in the previous studies. The v_d in Cases 4 and 5 are almost the same and did not significantly affect the difference of BCD rates (Figs. 2c, 5b, 5d, and 5f). This indicates that the effect of gravity settling effect is not so important for submicron size of BC particles. Case 6 by GOCART in the GEOS-4 calculated faster v_d than those by Cases 1, 2, 4, and 5 (Fig. 5). The faster v_d enhances BCD at the surface and simultaneously reduces the BCC in the atmosphere. It probably results in corresponding seemingly well to the background level of eqBCC observed at NCO-P site (Fig. 2a). In Case 6, the prescribed surface types were not ice surface at the NCO-P grid point, though there are Himalayan glaciers in the grid point (see Section 2.1, Fig. 1). The much greater surface roughness for non-ice surface compared to ice surface (see Table 1), will cause faster friction velocities leading to faster v_d which leads to larger amount of BCDs.

In addition, the calculated surface wind speed by GEOS-4 (Case 6), especially during nighttime, was faster than the observed one at NCO-P site (Fig. 6) probably due to the model representative height of wind speed. The NCO-P observed wind was at 3.5 m above ground level. However, the model used wind speed at the lowest layer (centered at about 50–60 m) to calculate v_d, which led to faster friction velocities and higher rate of BCD. That is probably why the GOCART's BCD is much higher than those in Cases 1, 2, 4, and 5. For Case 7 (SPRINTARS), although fluctuations of v_d were less than GOCART (Case 6), faster v_d compared to Cases 1, 2, 4, and 5 were also seen (Fig. 5). The wind speed at the lowest layer in SPRINTARS was also stronger and the surface roughness height was greater than that for ice surface (Table 1 and Fig. 6). As a result, the BCD by SPRINTARS was also much greater than Cases 1, 2, 4, and 5, and still greater than that of GOCART (Case 6). We carried out one additional sensitivity test so as to examine the impact of changing surface roughness height on v_d. For Case 3, the same calculation was carried out for Case 2, except for the surface roughness height. A great surface roughness of 1 m, corresponding to conifer forest, was used in this case (Table 1). Increasing the surface roughness will easily lead to a faster v_d and higher rate of BCD (Figs. 5and 2b). This is evident from the large difference in the v_d and BCD between Cases 2 and 3 (Fig. 5 and Table 2).

3.3. Differences of snow albedo reduction

In Table 2, the estimated BCDs of 266–4651 μg m^{-2} can be converted to the BCCs of 120.8–2114.2 (fresh snow with snow density of 110 kg m^{-3}) and 26.6–465.1 (old snow with snow density of 500 kg m^{-3}) μg kg^{-1} in 2-cm snow surface, respectively. There were larger differences on BCC in snow surface among different estimations of BCD in Cases 1–7 because of the differences in the amount of snow water equivalent. Note that the observed BCCs in snow over the Himalayas and TP are still limited (Kaspari et al., 2011; Ming et al., 2008, 2009; 2012; Xu et al., 2006, 2009a; 2009b), have a wider range and reveal many uncertainties (See SI). Our BCC estimates for both fresh and old snow are sometimes much higher than the observed BCC in snow at East Rongbuk Glacier (Northern side of the Himalayas) by Ming et al. (2008, 2009; 2012) and Kaspari et al. (2011). It indicates that, over the Himalayas, BCC in different snow conditions are highly variable. In addition, there are some possibilities that the amount of BCC in the snow at the southern slope would be higher than that at the northern slope (See SI). However, currently, we are unable to draw this conclusion because of the lack of BCC measurements in snow at the southern slope.

Next, we calculated broadband snow albedo reductions in VIS and NIR ranges (Table 3). The differences of the possible VIS snow albedo reductions between minimum and maximum among 7 cases for which all are considered as hydrophobic or hydrophilic BCs were 5.8 and 8.4% for fresh snow, and 5.5 and 7.9% for old snow, respectively. The reduction ranges in VIS and NIR albedos from pure snow albedos are approximately 1.2–10.9% and 0.2–3.0%, respectively (Table 3). The reductions in NIR were much smaller because of less absorption of the impurities (e.g., Warren and Wiscombe, 1980; Yasunari et al., 2011). In reality, snow metamorphism will also change snow albedo because of aging process on snow grain size (e.g., Wiscombe and Warren, 1980). Given the large range we considered between fresh and old snow albedos, it is likely that albedo change due to the process of snow metamorphism will lie somewhere in the range of our estimates of the fresh and old snow cover assumptions. However, a few percentage points in the change of snow albedo reduction would largely impact the glacier meltings during melting period (Yasunari et al., 2010). The albedo estimates have wider range and it is worth noting this. Hence, we should confirm or monitor this point in terms of in situ filed observations in future studies with the results of this study.

As discussed in Yasunari et al. (2010), the BCD of Case 1 may be "lower bound" and mostly not a true value in the real world. On the other hand, the BCD in Cases 6 and 7 may be much larger than actual values because of 1) stronger wind speed than that observed at the surface (Fig. 6) and 2) prescribed vegetated surface with greater roughness heights at the grid point, including NCO-P site, than that on the ice surface roughness over glaciers (Table 1). Although dry deposition theories used in many climate models still include many uncertainties (See SI), our estimation of BCD of 896–1333 μg m^{-2} during March–May 2006 (0.41–0.60 μg m^{-2} h^{-1}) (Cases 2, 4, and 5) with the ice surface assumption forced by met-data 1 are considered to be better (not absolutely accurate but probably closer) ranges than those by Cases 1, 3, 6, and 7. Hence, according to this study, most likely range of dry BCD and BCC in snow surface during March–May 2006 would probably exist within the ranges in Cases 2, 4, and 5 as shown in Table 2. More discussion would be necessary when there will be available future observations on BCC in snow at the southern slope. In addition, during the pre-monsoon period in 2006, we observed less precipitation (e.g., Bonasoni et al., 2008; Yasunari et al., 2010), a higher concentration of submicron aerosol particles, and more than 90% of total aerosol particle mass consisting of non-BC particles (Marinoni et al., 2010; Yasunari et al., 2010). This suggests that we can expect old aged snow conditions and an internal mixture of BC, such as sulfate-coated hydrophilic BC, because the old snow condition is considered to be the snow condition after metamorphism from fresh snow. Hence, Cases 2, 4, and 5 with hydrophilic BC and old snow with snow density of 500 kg m^{-3} could be our best guess uncertainty range on the snow albedos under diffuse sunlight condition or at solar zenith angle of 50° during the pre-monsoon in 2006 (Table 3).

4. Conclusion

In this work, we have estimated the possible uncertainty range of BCDs from different v_d and global model outputs. The estimated possible range on BCD and related snow albedo reductions are important in both atmospheric chemistry and climate studies for the Himalayan region. We hope to provide useful data on BCD discussion over Himalayan glaciers due to the significant emissions of BC from open biomass burning and other anthropogenic sources in the region. Currently we do not intend to and cannot, determine the accurate BCD values and snow albedo reductions because there are no observations in details at the southern slope of the Himalayas for comparison and validation. However, we were able to determine the possible range of BCD and its snow albedo reductions over Himalayan glaciers at this stage of our study. Our results suggest that incorrect specification of surface roughness type such as vegetated surface over the grid point, including glaciers and strong surface wind in regional or global model, cause faster v_d and larger amounts BCD over the glaciers. Hence, surface roughness parameter and wind speed are the most critical factor in determining the BCD rates over Himalayan glaciers. The differences arising from BCD rates will eventually lead to further, wider differences on the estimates of glacier retreats over Himalayan and Tibetan regions in global or regional modeling studies. How to estimate v_d more accurately at the grid point, which includes snow cover or glacier surface, is the key to assess glacier retreats or seasonal snow melt timings, in terms of the debris-covered area, snow darkening effect due to climate and environmental changes, using climate models. Model projections on glacier retreat, need to include estimates of uncertainties from key factors contributing to glacial mass balance change such as precipitation, wind, debris-covered area, snow aging, solar absorbing impurities in snow (i.e., BC, dust, organic matters, and snow algae), anthropogenic effects from atmospheric heating by the absorbing aerosols, and global warming (e.g., Takeuchi et al., 2001; IPCC, 2007; Flanner et al., 2007, 2009; Fujita, 2008; Lau et al., 2010; Scherler et al., 2011; Yasunari et al., 2011; Aoki et al., 2011).

Furthermore, the discussion on the contribution of dust mentioned above to the glacial phenomenon studied here is an important consideration for future works. However, we separated the aspect of dust from our study to assure clarity. Confronting the Himalayan glacier issue step by step, we focused solely on the "dry deposition", rather than wet deposition, because it dominates the pre-monsoon period. In this study we provided an estimate of the possible uncertainty range on the amount of BCD and its relevant snow albedo reductions from different estimation methods. Future studies, including in situ observations integrated with the outcomes from this study, would hopefully reduce the uncertainties on BCD. We trust that this study will be helpful for future research on regional and global aerosol modeling over snowfall regions, as well as useful to those scientists working on snow-related issues.

Acknowledgment

All the observed data in the atmosphere at NCO-P site were maintained by the framework of the Ev-K2-CNR "SHARE", UNEP "ABC" and PAPRIKA (ANR-EVK2CNR) projects. This research is conducted under the Joint Aerosol Monsoon Experiment (JAMEX). The first author was on a visiting fellowship to the Goddard Earth Science and Technology Center (GEST) at the University of Maryland at Baltimore County (UMBC, NASA Grant and Cooperative Agreement NCC5-494) and is currently on the fellowship to Goddard Earth Sciences Technology and Research (GESTAR), Universities Space Research Association (USRA, NASA Grant and Cooperative Agreement NNG11HP08). The MODIS data used in this paper were produced with the Giovanni online data system, developed and maintained by the NASA GES DISC. The authors gratefully acknowledge the NOAA Air Resources Laboratory (ARL) for the provision of the HYSPLIT transport and dispersion model and/or READY website (http://www.arl.noaa.gov/ready.php) used in this publication. We really appreciate Jan Angevine, at NASA Goddard Space Flight Center, for proofreading our paper.

Appendix A. Supplementary data

Supplementary data related to this article can be found online at doi:10.1016/j.atmosenv.2012.03.031.

References

Aoki, Te., Kuchiki, K., Niwano, M., Kodama, Y., Hosaka, M., Tanaka, T., 2011. Physically based snow albedo model for calculating broadband albedos and the solar heating profile in snowpack for general circulation models. Journal of Geophysical Research 116, D11114. doi:10.1029/2010JD015507.

Bonasoni, P., Laj, P., Angelini, F., Arduini, J., Bonafè, U., Calzolari, F., Cristofanelli, P., Decesari, S., Facchini, M.C., Fuzzi, S., Gobbi, G.P., Maione, M., Marinoni, A., Petzold, A., Roccato, F., Roger, J.C., Sellegri, K., Sprenger, M., Venzac, H., Verza, G.P., Villani, P., Vuillermoz, E., 2008. The ABC-pyramid Atmospheric Research Observatory in Himalaya for aerosol, ozone and halocarbon measurements. Science of the Total Environment 391 (2–3), 252–261.

Bonasoni, P., Laj, P., Marinoni, A., Sprenger, M., Angelini, F., Arduini, J., Bonafè, U., Calzolari, F., Colombo, T., Decesari, S., Di Biagio, C., di Sarra, A.G., Evangelisti, F., Duchi, R., Facchini, M.C., Fuzzi, S., Gobbi, G.P., Maione, M., Panday, A., Roccato, F., Sellegri, K., Venzac, H., Verza, G.P., Villani, P., Vuillermoz, E., Cristofanelli, P., 2010. Atmospheric brown clouds in the Himalayas: first two years of continuous observations at the Nepal-climate Observatory at Pyramid (5079 m). Atmospheric Chemistry and Physics 10, 7515–7531.

Bond, T.C., Streets, D.G., Yarber, K.F., Nelson, S.M., Woo, J.-H., Klimont, Z., 2004. A technology-based global inventory of black and organic carbon emissions from combustion. Journal of Geophysical Research 109, D14203. doi:10.1029/2003JD003697.

Bond, T.C., Bergstrom, R.W., 2006. Light absorption by carbonaceous particles: an investigative review. Aerosol Science and Technology 40, 27–67.

Chin, M., Ginoux, P., Kinne, S., Holben, B.N., Duncan, B.N., Martin, R.V., Logan, J.A., Higurashi, A., Nakajima, T., 2002. Tropospheric aerosol optical thickness from the GOCART model and comparisons with satellite and sunphotometer measurements. Journal of the Atmospheric Sciences 59, 461–483.

Chin, M., Diehl, T., Dubovik, O., Eck, T.F., Holben, B.N., Sinyuk, A., Streets, D.G., 2009. Light absorption by pollution, dust, and biomass burning aerosols: a global model study and evaluation with AERONET measurements. Annales Geophysicae 27, 3439–3464.

Cong, Z., Kang, S., Qin, D., 2009. Seasonal features of aerosol particles recorded in snow from Mt. Qomolangma (Everest) and their environmental implications. Journal of Environmental Science 21 (7), 914–919.

Cong, Z., Kang, S., Dong, S., Liu, X., Qin, D., 2010. Elemental and individual particle analysis of atmospheric aerosols from high Himalayas. Environmental Monitoring and Assessment 160, 323–335. doi:10.1007/s10661-008-0698-3.

Draxler, R.R., Rolph, G.D., 2011. HYSPLIT (HYbrid Single-Particle Lagrangian Integrated Trajectory) Model access via NOAA ARL READY. NOAA Air Resources Laboratory, Silver Spring, MD. Website: http://ready.arl.noaa.gov/HYSPLIT.php (accessed 01.03.12.).

Flanner, M.G., Zender, C.S., Randerson, J.T., Rasch, P.J., 2007. Present-day climate forcing and response from black carbon in snow. Journal of Geophysical Research 112 (D11), D11202. doi:10.1029/2006JD008003.

Flanner, M.G., Zender, C.S., Hess, P.G., Mahowald, N.M., Painter, T.H., Ramanathan, V., Rasch, P.J., 2009. Springtime warming and reduced snow cover from carbonaceous particles. Atmospheric Chemistry and Physics 9 (7), 2481–2497.

Fujita, K., 2008. Effect of precipitation seasonality on climatic sensitivity of glacier mass balance. Earth and Planetary Science Letters 276 (1-2), 14–19.

Fujita, K., Ageta, Y., 2000. Effect of summer accumulation on glacier mass balance on the Tibetan Plateau revealed by mass-balance model. Journal of Glaciology 46 (153), 244–252.

Holland, D.M., 2000. Merged IBCAO/ETOPO5 Global Topographic Data Product. National Geophysical Data Center (NGDC), Boulder Colorado. Available online at: http://efdl.cims.nyu.edu/project_aomip/forcing_data/topography/merged/overview.html (accessed 01.03.12.).

IPCC, 2007. Summary for Policymakers. In: Solomon, S., Qin, D., Manning, M., Chen, Z., Marquis, M., Averyt, K.B., Tignor, M., Miller, H.L. (Eds.), Climate Change 2007: The Physical Science Basis. Contribution of Working Group I to the Fourth Assessment Report of the Intergovernmental Panel on Climate Change. Cambridge University Press, Cambridge, United Kingdom\New York, NY, USA.

Kaspari, S.D., Schwikowski, M., Gysel, M., Flanner, M.G., Kang, S., Hou, S., Mayewski, P.A., 2011. Recent increase in black carbon concentrations from a Mt. Everest ice core spanning 1860–2000 AD. Geophysical Research Letters 38, L04703. doi:10.1029/2010GL046096.

Lau, K.M., Kim, M.K., Kim, K.M., 2006. Asian summer monsoon anomalies induced by aerosol direct forcing: the role of the Tibetan Plateau. Climate Dynamics 26 (7–8), 855–864.
Lau, K.M., Kim, K.M., 2006. Observational relationships between aerosol and Asian monsoon rainfall, and circulation. Geophysical Research Letters 33. doi:10.1029/2006GL027546.
Lau, K.-M., Ramanathan, V., Wu, G., Li, Z., Tsay, S.C., Hsu, C., Sikka, R., Holben, B., Lu, D., Tartari, G., Chin, M., Koudelova, P., Chen, H., Ma, Y., Huang, J., Taniguchi, K., Zhang, R., 2008. The joint aerosol-monsoon experiment: a new challenge in monsoon climate research. Bulletin of the American Meteorological Society 89 (3), 369–383. doi:10.1175/BAMS-89-3-369.
Lau, K.M., Kim, M.K., Kim, K.M., 2010. Enhanced surface warming and accelerated snow melt in the Himalayas and Tibetan Plateau induced by absorbing aerosols. Environmental Research Letters 5, 025204. doi:10.1088/1748-9326/5/2/025204.
Marcq, S., Laj, P., Roger, J.C., Villani, P., Sellegri, K., Bonasoni, P., Marinoni, A., Cristofanelli, P., Verza, G.P., Bergin, M., 2010. Aerosol optical properties and radiative forcing in the high Himalaya based on measurements at the Nepal Climate Observatory-Pyramid site (5079 m a.s.l.). Atmospheric Chemistry and Physics 10, 5859–5872. doi:10.5194/acp-10-5859-2010.
Marinoni, A., Cristofanelli, P., Laj, P., Duchi, R., Calzolari, F., Decesari, S., Sellegri, K., Vuillermoz, E., Verza, G.P., Villani, P., Bonasoni, P., 2010. Aerosol mass and black carbon concentrations, a two year record at NCO-P (5079 m, Southern Himalayas). Atmospheric Chemistry and Physics 10, 8551–8562. doi:10.5194/acp-10-8551-2010.
Menon, S., Koch, D., Beig, G., Sahu, S., Fasullo, J., Orlikowski, D., 2010. Black carbon aerosols and the third polar ice cap. Atmospheric Chemistry and Physics 10, 4559–4571.
Ming, J., Cachier, H., Xiao, C., Qin, D., Kang, S., Hou, S., Xu, J., 2008. Black carbon record based on a shallow Himalayan ice core and its climatic implications. Atmospheric Chemistry and Physics 8 (5), 1343–1352.
Ming, J., Xiao, C., Cachier, H., Qin, D., Qin, X., Li, Z., Pu, J., 2009. Black carbon (BC) in the snow of glaciers in west China and its potential effects on albedos. Atmospheric Research 92 (1), 114–123.
Ming, J., Du, Z., Xiao, C., Xu, X., Zhang, D., 2012. Darkening of the mid-Himalaya glaciers since 2000 and the potential causes. Environmental Research Letters 7, 014021. doi:10.1088/1748-9326/7/1/014021.
Naoe, H., Hasagawa, S., Heintzenberg, J., Okada, K., Uchiyama, A., Zaizen, Y., Kobayashi, E., Yamazaki, A., 2009. State of mixture of atmospheric submicrometer black carbon particles and its effect on particulate light absorption. Atmospheric Environment 43, 1296–1301. doi:10.1016/j.atmosenv.2008.11.031.
Nho-Kim, E.-Y., Michou, M., Peuch, V.-H., 2004. Parameterization of size-dependent particle dry deposition velocities for global modelling. Atmospheric Environment 38, 1933–1942.
Qian, Y., Gustafson Jr., W.I., Leung, L.R., Ghan, S.J., 2009. Effects of soot-induced snow albedo change on snowpack and hydrological cycle in western United States based on weather research and forecasting chemistry and regional climate simulations. Journal of Geophysical Research 114, D03108. doi:10.1029/2008JD011039.
Qian, Y., Flanner, M.G., Leung, L.R., Wang, W., 2011. Sensitivity studies on the impacts of Tibetan Plateau snowpack pollution on the Asian hydrological cycle and monsoon climate. Atmospheric Chemistry and Physics 11, 1929–1948. doi:10.5194/acp-11-1929-2011.
Ramanathan, V., Li, F., Ramana, M.V., Praveen, P.S., Kim, D., Corrigan, C.E., Nguyen, H., Stone, E.A., Schauer, J.J., Carmichael, G.R., Adhikary, B., Yoon, S.C., 2007. Atmospheric brown clouds: hemispherical and regional variations in long-range transport, absorption, and radiative forcing. Journal of Geophysical Research 112, D22S21. doi:10.1029/2006JD008124.
Ramanathan, V., Carmichael, G., 2008. Global and regional climate changes due to black carbon. Nature Geoscience 1, 95–100.
Redemann, J., Russell, P.B., Hamill, P., 2001. Dependence of aerosol light absorption and single-scattering albedo on ambient relative humidity for sulfate aerosols with black carbon cores. Journal of Geophysical Research 106 (D21), 27485–27495.
Rolph, G.D., 2011. Real-time Environmental Applications and Display sYstem (READY). NOAA Air Resources Laboratory, Silver Spring, MD. Website: http://ready.arl.noaa.gov (accessed 01.03.12.).
Scherler, D., Bookhagen, B., Strecker, M.R., 2011. Spatially variable response of Himalayan glaciers to climate change affected by debris cover. Nature Geoscience 4, 156–159. doi:10.1038/ngeo1068.
Schwarz, J.P., Spackman, J.R., Fahey, D.W., Gao, R.S., Lohmann, U., Stier, P., Watts, L.A., Thomson, D.S., Lack, D.A., Pfister, L., Mahoney, M.J., Baumgardner, D., Wilson, J.C., Reeves, J.M., 2008. Coatings and their enhancement of black carbon light absorption in the tropical atmosphere. Journal of Geophysical Research 113, D03203. doi:10.1029/2007JD009042.
Takemura, T., Okamoto, H., Maruyama, Y., Numaguti, A., Higurashi, A., Nakajima, T., 2000. Global three-dimensional simulation of aerosol optical thickness distribution of various origins. Journal of Geophysical Research 105, 17853–17873.
Takemura, T., Nakajima, T., Dubovik, O., Holben, B.N., Kinne, S., 2002. Single-scattering albedo and radiative forcing of various aerosol species with a global three-dimensional model. Journal of Climate 15, 333–352.
Takeuchi, N., Kohshima, S., Seko, K., 2001. Structure, formation, and darkening process of albedo-reducing material (cryoconite) on a Himalayan Glacier: a granular algal mat growing on the glacier. Arctic, Antarctic, and Alpine Research 33 (2), 115–122.
Tedesco, M., Kelly, R.E.J., Foster, J.L., Chang, A.T.C., 2004. Updated Monthly. AMSR-E/Aqua Monthly L3 Global Snow Water Equivalent EASE-Grids V002, March to May 2006 Data Used. National Snow and Ice Data Center, Boulder, Colorado USA. Digital media: http://nsidc.org/data/docs/daac/ae_swe_ease-grids.gd.html (accessed 01.03.12.).
Walcek, C.J., Brost, R.A., Chang, J.S., Wesely, M.L., 1986. SO_2, sulfate and HNO_3 deposition velocities computed using regional land use and meteorological data. Atmospheric Environment 20, 949–964.
Warren, S.G., Wiscombe, W.J., 1980. A model for the Spectral albedo of snow. 2. Snow containing atmospheric aerosols. Journal of the Atmospheric Sciences 37 (12), 2734–2745.
Wesely, M.L., 1989. Parameterization of surface resistance to gaseous dry deposition in regional-scale numerical models. Atmospheric Environment 23, 1293–1304.
Wiscombe, W.J., Warren, S.G., 1980. A model for the spectral albedo of snow, I: Pure snow. Journal of the Atmospheric Sciences 37 (12), 2712–2733.
Xu, B., Yao, T., Liu, X., Wang, N., 2006. Elemental and organic carbon measurements with a two-step heating-gas chromatography system in snow samples from the Tibetan Plateau. Annals of Glaciology 43, 257–262.
Xu, B., Wang, M., Joswiak, D.R., Cao, J., Yao, T., Wu, G., Yang, W., Zhao, H., 2009a. Deposition of anthropogenic aerosols in a southeastern Tibetan glacier. Journal of Geophysical Research 114, D17209. doi:10.1029/2008JD011510.
Xu, B., Cao, J., Hansen, J., Yao, T., Joswia, D.R., Wang, N., Wu, G., Wang, M., Zhao, H., Yang, W., Liu, X., He, J., 2009b. Black soot and the survival of Tibetan glaciers. Proceedings of the National Academy of Sciences of the United States of America 106 (52), 22114–22118. doi:10.1073/pnas.0910444106.
Yasunari, T.J., Bonasoni, P., Laj, P., Fujita, K., Vuillermoz, E., Marinoni, A., Cristofanelli, P., Duchi, R., Tartari, G., Lau, K.M., 2010. Preliminary estimation of black carbon deposition from Nepal Climate Observatory – Pyramid data and its possible impact on snow albedo changes over Himalayan glaciers during the pre-monsoon season. Atmospheric Chemistry and Physics 10, 6603–6615. doi:10.5194/acp-10-6603-2010.
Yasunari, T.J., 2011. What influences climate and glacier change in the southwestern China? Environmental Research Letters 6, 041001. doi:10.1088/1748-9326/6/4/041001.
Yasunari, T.J., Koster, R.D., Lau, K.M., Aoki, Te, Sud, Y.C., Yamazaki, T., Motoyoshi, H., Kodama, Y., 2011. Influence of dust and black carbon on the snow albedo in the NASA Goddard Earth Observing System version 5 land surface model. Journal of Geophysical Research 116, D02210. doi:10.1029/2010JD014861.